PHYSICAL REVIEW C **93**, 021601(R) (2016)

Structure of ^{107}Sn studied through single-neutron knockout reactions

G. Cerizza,[1,*] A. Ayres,[1] K. L. Jones,[1] R. Grzywacz,[1] A. Bey,[1] C. Bingham,[1] L. Cartegni,[1] D. Miller,[1,†] S. Padgett,[1,‡] T. Baugher,[2,§] D. Bazin,[2] J. S. Berryman,[2] A. Gade,[2] S. McDaniel,[2] A. Ratkiewicz,[2,‡] A. Shore,[2] S. R. Stroberg,[2,‖] D. Weisshaar,[2] K. Wimmer,[2,¶] R. Winkler,[2] S. D. Pain,[3] K. Y. Chae,[3,**] J. A. Cizewski,[4] M. E. Howard,[4] and J. A. Tostevin[5]

[1]*Department of Physics and Astronomy, University of Tennessee, Knoxville, Tennessee 37996, USA*

[2]*National Superconducting Cyclotron Laboratory and Department of Physics and Astronomy, Michigan State University, East Lansing, Michigan 48824, USA*

[3]*Physics Division, Oak Ridge National Laboratory, Oak Ridge, Tennessee 37831, USA*

[4]*Department of Physics and Astronomy, Rutgers University, New Brunswick, New Jersey 08903, USA*

[5]*Department of Physics, University of Surrey, Guildford, Surrey GU2 7XH, United Kingdom*

(Received 21 August 2015; published 4 February 2016)

The neutron-deficient nucleus ^{107}Sn has been studied by using the one-neutron knockout reaction. By measuring the decay γ rays and momentum distributions of reaction residues, the spins of the ground, $5/2^+$, and first-excited, $7/2^+$, states of ^{107}Sn have been assigned by comparisons to eikonal-model reaction calculations. Limits on the inclusive and exclusive cross sections have been measured and transitions due to neutron removals from below the $N = 50$ closed shell have been observed. New excited states up to 5.5 MeV in ^{107}Sn have been identified.

DOI: 10.1103/PhysRevC.93.021601

The structure of the atomic nucleus is influenced by the filling of shells with neutrons and protons, analogous to electronic shells in the atom. These structures have been well studied around the stable magic nuclei ^{16}O, ^{40,48}Ca, and ^{208}Pb [1] as a testing ground for nuclear models. However, away from stability, where nuclei have short lifetimes and are difficult to produce and study, the properties of exotic doubly magic nuclei, such as ^{78}Ni [2,3] and ^{100}Sn [4,5], are less known. Nuclei around ^{100}Sn are important for nuclear structure studies away from stability owing to the shell closures at $N = Z = 50$, as well as their proximity to the $N = Z$ line. The region is also at the end of the astrophysical rapid proton capture (rp) process [6]. There has been intense recent effort to measure collective properties of light tin nuclei through Coulomb excitation [7–9]. Complementary to those studies, the ordering and nature of the single-particle states in this region can be investigated by using intermediate-energy nucleon-removal reactions. According to the shell model, the lowest-lying neutron single-particle states above ^{100}Sn correspond to the second $d_{5/2}$ and the first $g_{7/2}$ orbitals. These orbitals are nearly degenerate, as measured in ^{101}Sn [10], where they are separated by just 172 (2) keV. In that study, the assumed ordering of these ^{101}Sn states, with the $5/2^+$ state below the $7/2^+$, could only be reproduced by reducing the shell-model $(g_{7/2})^2_{J=0}$ matrix element by about 30% [10].

A study by Darby *et al.* [11] populated ^{101}Sn through the ^{109}Xe $\rightarrow$ ^{105} Te $\rightarrow$ ^{101} Sn α chain. This revealed a large branching ratio, $I_\alpha = 89(4)\%$, from the ^{105}Te ground state to the ^{101}Sn first-excited state, suggesting that (i) the spins of these two states are the same, and (ii) the spins of the ground states differ. Supported by state-of-the-art shell-model configuration interaction (CI) calculations, Darby *et al.* concluded that the ^{101}Sn ground state has $J^\pi = 7/2^+$, while the first-excited state has $J^\pi = 5/2^+$. This implies that the single-particle $g_{7/2}$ state is below the $d_{5/2}$ state, contrary to previous expectations. A model calculation in Ref. [11] also suggested that enhanced binding from the $(g_{7/2})^2_{J=0} \otimes d_{5/2}$ configuration in ^{103}Sn leads to mixed configurations in the odd-mass, light tin isotopes where, naïvely, pure $(g_{7/2})^3$ or $(d_{5/2})^3$ configurations might be expected to dominate.

Intermediate-energy one-nucleon knockout reactions present an excellent method for extracting nuclear structure information from low-intensity radioactive ion beams [12–14]. The shape of the momentum distributions of the reaction residues are dependent on the orbital angular momentum of the removed nucleon. Additionally, the partial cross sections to specific final states carry spectroscopic information on the wave function of the projectile. Neutron knockout reactions have been used mostly for light and medium-heavy nuclei. For heavier nuclei, the separation of the projectile beam passing through the target and the one-neutron knockout residues becomes more difficult. Here we present the first neutron knockout reaction measurement in the $Z = 50$ region.

A 140 MeV/u ^{124}Xe primary beam was accelerated with the coupled cyclotrons of the National Superconducting

*Current address: National Superconducting Cyclotron Laboratory and Department of Physics and Astronomy, Michigan State University, East Lansing, Michigan 48824, USA.

†Current address: Idaho National Laboratory, Idaho Falls, Idaho 83415, USA.

‡Current address: Lawrence Livermore National Laboratory, Livermore, California 94550, USA.

§Current address: Department of Physics and Astronomy, Rutgers University, New Brunswick, New Jersey 08903, USA.

‖Current address: TRIUMF, Vancouver, British Columbia, Canada V6T 2A3C.

¶Current address: University of Tokyo, Hongo, Bunkyo-ku, Tokyo 113-0033, Japan.

**Current address: Department of Physics, Sungkyunkwan University, Suwon 440-746, Korea.

Cyclotron Laboratory at Michigan State University. Two settings of the A1900 fragment separator [15] were used to select ^{108}Sn and ^{106}Sn secondary beams and to deliver them to the target position of the S800 spectrograph [16]. The momentum acceptance was set to 0.3% in order to provide beams of ^{108}Sn and ^{106}Sn with purities of 1.9% and 0.14%, respectively. A thin plastic scintillator located at the A1900 focal plane was used in conjunction with a downstream scintillator to measure the time of flight of the particles, allowing us to identify the different species in the entrance channel on an event-by-event basis. The high levels of contamination originate from low-momentum tails of higher-rigidity fragments that overlap with the momentum acceptance of the fragment separator [17]. The major contaminant species were $^{107(105)}$In and $^{106(104)}$Cd for the $^{108(106)}$Sn settings. The secondary tin beams impinged on a 47 mg/cm^2 ^{9}Be reaction target at the target position of the S800 magnetic spectrometer with an energy of ≈80 MeV/u. The average rates on the reaction target for ^{108}Sn and ^{106}Sn were 3000 and 100 pps, respectively.

The secondary target was surrounded by the high-efficiency CsI(Na) scintillator array (CAESAR) [18] that was used to identify the decay γ rays of the reaction products. CAESAR consists of 192 CsI(Na) crystals with 95% of solid-angle coverage. The granularity of the array enables event-by-event Doppler reconstruction of γ rays emitted in-flight. The detection efficiency of the array was determined with ^{88}Y, ^{22}Na, ^{137}Cs, ^{133}Ba, and ^{60}Co calibration standards. To model the in-beam spectral response of CAESAR (30% full-energy peak efficiency at 1 MeV), GEANT4 [19] simulations were performed and benchmarked with source data. In the analysis, nearest-neighbor addback was used to analyze Compton-scattered photons with the effect of increasing the detection efficiency.

The reaction residues were identified event by event by using the time of flight (TOF) between two plastic scintillators and the energy loss (ΔE) measured in the S800 focal-plane ion chamber (IC). The particle-identification spectrum for the reactions induced by the ^{108}Sn beam are shown in Fig. 1 for events where at least one γ ray was observed. In total, 17 000 ^{107}Sn and 3000 ^{105}Sn candidate events were measured in approximately two days of run time per beam setting. Two cathode readout drift chambers (CRDCs) measured the particle positions and angles in the focal plane. These were used to reconstruct the momentum distributions of the reaction residues.

Here, we present the results of one-neutron knockout from the ^{108}Sn beam. For ^{106}Sn, the low-statistics results are published in Ref. [20]. Figure 2 shows the γ-ray spectrum for the ^{108}Sn beam measured in coincidence with the ^{107}Sn reaction residues. The blue (solid) line shows a χ^2 fit of the GEANT4 simulation using known transitions in ^{107}Sn. The ^{107}Sn first excited state at 151.2 keV is clearly visible.

The full momentum vector of the ^{107}Sn fragments was reconstructed event by event. Position and angle information from the CRDCs was combined with trajectory reconstruction through the spectrograph by using the COSY INFINITY [21] code, to reconstruct the longitudinal momentum distributions at the target position. The width of the longitudinal-momentum distribution is sensitive to the orbital-angular-momentum quantum number of the removed nucleon. The momentum

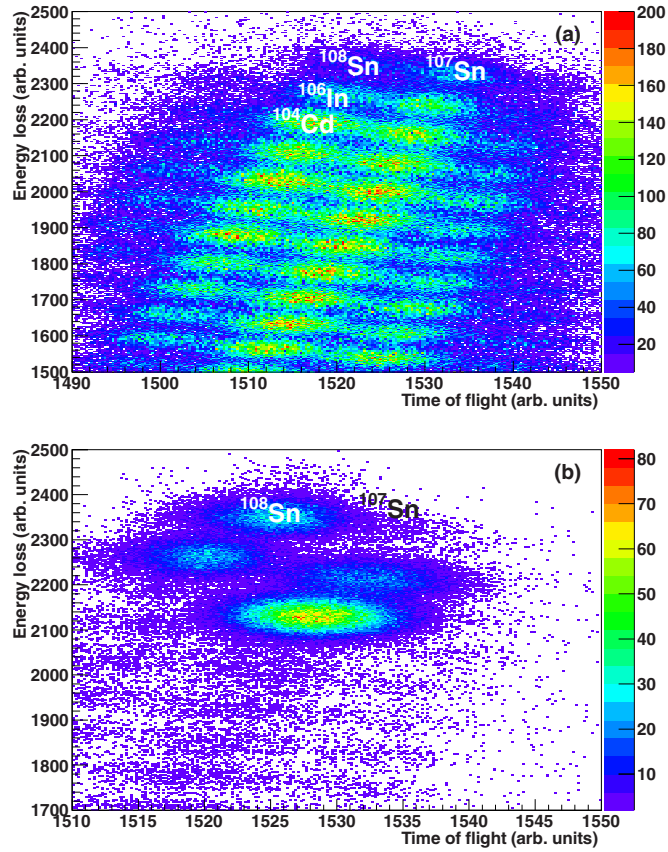

FIG. 1. Particle-identification spectrum for the reaction products of the ^{108}Sn beam passing through the ^{9}Be target. The energy loss measured in the ion chamber is plotted versus the ion's flight time with the requirements of γ-particle (top) and only particle (bottom) coincidence. For the latter case, the particle single trigger was downscaled by a factor of 10. Several other isotopes have been produced and identified via γ spectroscopy, such as ^{106}In and ^{104}Cd.

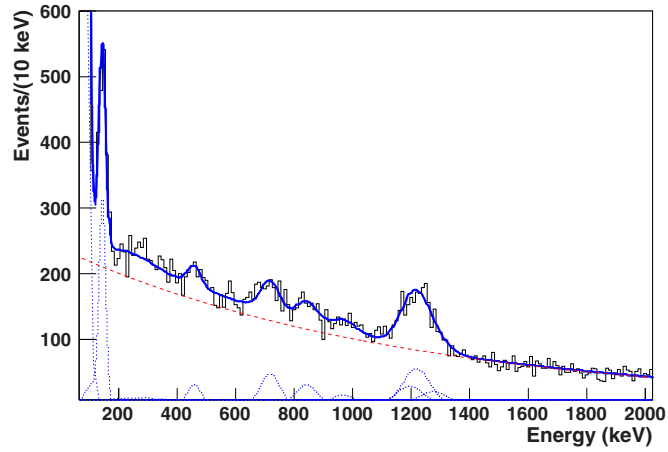

FIG. 2. Spectrum of γ rays following neutron removal from a ^{108}Sn beam, gated on ^{107}Sn residual nuclei. The blue (solid) line shows a fit to the data; in light blue (dotted) the GEANT4 simulation of the CAESAR detector for the observed γ transitions; the exponential background is shown as a red (dashed) line.

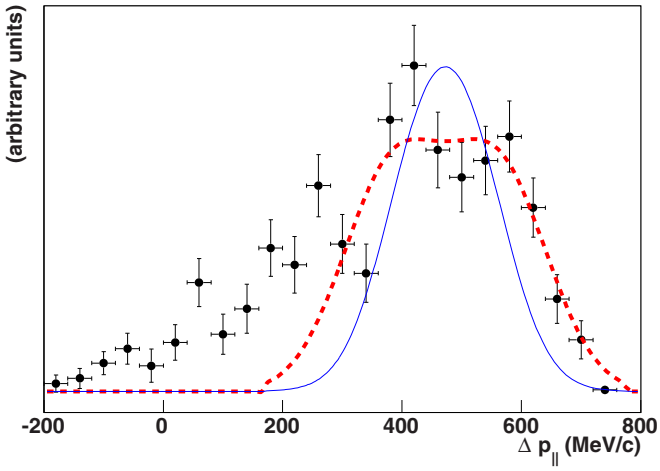

FIG. 3. Momentum distributions of the ^{107}Sn reaction residues in the first-excited state. The data are overlaid to eikonal model reaction calculations for neutron removal from a $2d_{5/2}$ orbital (blue solid) and a $1g_{7/2}$ orbital (red dashed).

distribution of residues produced in the ^{107}Sn first excited state is shown in Fig. 3. This has been obtained by reconstructing the momentum distribution of the energy region around the 151 keV peak of Fig. 2 and subtracting the weighted contributions from the background and from the population of higher-lying states according to the known feeding scheme and fit results. For the ^{107}Sn ground state, an unambiguous determination of the correct shape of the momentum distribution was not possible owing to the unreacted beam that reached the S800 focal plane. Weaker, unreacted-beam contaminants, not resolvable by the incoming particle selection, pass without emitting γ rays (i.e., unreacted) through the reaction target, competing in intensity with the ^{107}Sn reaction products and ending up in their vicinity in the particle-identification spectrum. Because these contaminants are unreacted, only excited reaction products like ^{107}Sn can satisfy the γ-particle coincidence condition, explaining the cleaning effect on the particle identification spectrum of the top of Fig. 1, when presence of the γ rays is requested. This issue will be reflected in the measurement of the inclusive one-neutron-removal cross section where only an upper limit will be provided.

The results of eikonal model reaction calculations, after convolution with an experimental resolution of 75 MeV/c are overlaid on Fig. 3. The details of the methods, geometries, and interactions used can be found in Refs. [12,22]. The curves show the calculated distributions when assuming neutron removal, with the physical separation energies, from an $\ell = 2$ (blue solid) or $\ell = 4$ (red dashed) orbital. For the first-excited-state transition, the $\ell = 4$ scenario better represents the width of the momentum distribution, especially on the high-momentum side. This is confirmed by a χ^2 fit to the data assuming each hypothesis. When compared to the knockout calculations, the data reveal an excess of events on the low-momentum side where more-dissipative, energy-sharing events with the target have been shown to broaden the momentum distribution [23]. We conclude that the ^{107}Sn first-excited state results from $g_{7/2}$ neutron removal and, by exclusion, the ^{107}Sn ground state from $d_{5/2}$ neutron removal. We assign $J^\pi = 5/2^+$ and $J^\pi = 7/2^+$ to the ground and first-excited states, respectively.

In a spectator-core approximation of direct neutron removal (i.e., fast reactions that leave the $A - 1$ system intact), the cross sections for populating particle-bound residue final states are dependent on the separation energy of the removed neutron. If in ^{108}Sn the eight valence neutrons were restricted to the $2d_{5/2}$ and $1g_{7/2}$ orbitals above the $N = 50$ shell closure, it is reasonable to expect that these orbitals will contribute significantly to low-lying final states. However, there are many neutrons occupying orbitals just below the shell gap, the removal of which will populate highly excited ^{107}Sn residues. In the region around ^{100}Sn the shell gap is ≈6.4 MeV [24], which quantifies the likely excitation energies of final states resulting from removal of neutrons from below $N = 50$. Those states which are particle bound and have a large γ-decay branch will decay either via high-energy γ rays or via a cascade of coincident lower-energy γ rays. The present γ detection system was optimized for low-energy γ rays to detect decays from the first-excited state in ^{107}Sn. The CAESAR detector was used at a dynamic range of 8 MeV with energy trigger thresholds of about 80 keV set crystal by crystal. As an immediate consequence, the number of low-energy γ rays from target-nucleus interactions increased, as can be seen in the lower part of the energy spectrum of Fig. 2. There are known transitions in ^{107}Sn above the first-excited state, which are clearly observed following the reaction—most notably a wide bump at around 1220 keV. The width of this bump is due to the combined effect of the Doppler broadening and the clustering of several transitions with energies between 1200 and 1300 keV. These are known excited states that decay either directly to the ground state or through the first-excited state, with unconfirmed spin values between 3/2 and 11/2. By using CAESAR as a calorimeter, i.e., summing all the Doppler-corrected γ rays with addback for each event, we can extract additional information, as shown in Fig. 4, for events with a γ multiplicity of less than or equal to three. In this spectrum, it is possible to separate and identify two doublets out of the 1200 keV bump of Fig. 2 and utilize an alternative method for γ-γ coincidences. The area of interest has been expanded in Fig. 5: the resolution of the peaks in the data (black solid line) are well described by the GEANT4 simulation (red dashed line) with the exception of the region around 1100 keV where additional, unknown levels may exist. The presence of low-energy γ rays owing to the crystal threshold settings has only a small impact on the calorimeter spectrum. These events have low multiplicities and energies that would add up at most to 500 keV.

Even though the simulated efficiency for measuring γ rays above 4 MeV is 15% to 20%, previously unknown highly excited states and γ cascades have been observed by using the calorimeter spectrum to gate the Doppler-corrected-singles data. An example of this technique is shown in the top-right frame of Fig. 4 where the singles spectrum, gated on the calorimeter energy in the 5400–5600 keV range, is plotted for multiplicity two. Two individual γ rays in coincidence have been observed around 1280 and 4200 keV and identified as the decay of a previously unobserved highly excited state around

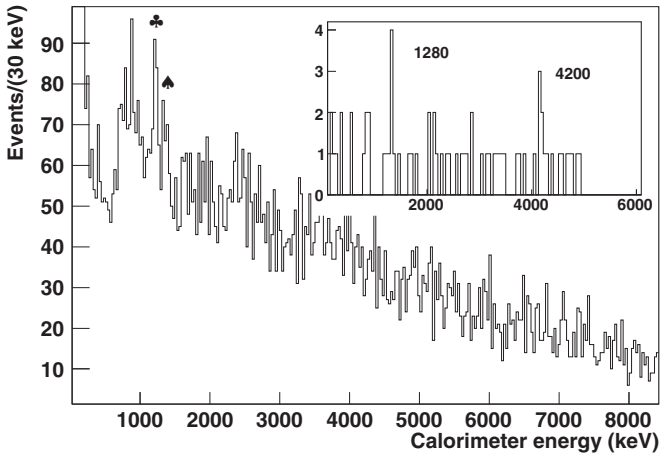

FIG. 4. CAESAR calorimeter distribution between 25 and 8425 keV. The 1222–1280 keV (club) and 1349–1370 keV (spade) multiplets are marked. The top-right inset shows an example of a singles spectrum gated on the calorimeter energy in the 5400–5600 keV range. Two distinct peaks above the background events are visible around 1280 and 4200 keV.

5500 keV. This demonstrates an advantage over traditional γ-γ coincidence techniques. Neither the 1280 nor the 4200 keV γ ray was individually distinguishable in the ungated singles spectrum. The 1280 keV γ is part of a multiplet peak, as shown in Fig. 2, while the 4200 keV γ has low statistics because of the detection efficiency at high energies. The results obtained with this technique were used to extend the level scheme, which is shown in Fig. 6. We propose that these highly excited states were populated via the removal of $1g_{9/2}$ neutrons from below the $N = 50$ closed shell.

Inclusive cross-section measurements for one-neutron removal and partial cross sections to low-lying states in ^{107}Sn are shown in Table I. We compare these with eikonal-model

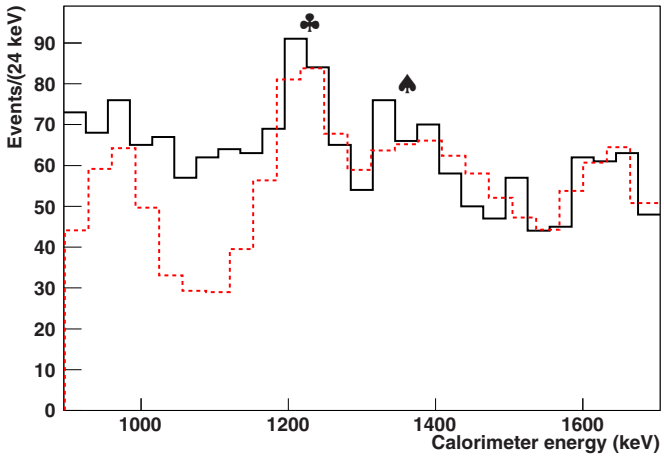

FIG. 5. CAESAR calorimeter distribution between 900 and 1700 keV. The 1222–1280 keV (club) and 1349–1370 keV (spade) multiplets are marked. Here, the data (black solid line) and the GEANT4 simulation (red dashed line) are compared: the expected and the measured resolution for the two peaks of interest are in good agreement.

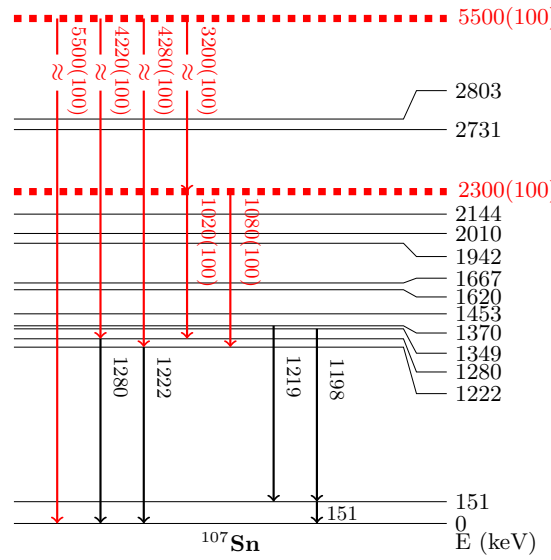

FIG. 6. Proposed level scheme for ^{107}Sn. New highly excited states (red dashed lines) have been observed cascading directly into the ground and excited states (red arrows). The experimental resolution of these new levels is estimated to be about 100 keV.

reaction calculations [13,14,25] using shell-model structure input. The spectroscopic factors C^2S were calculated with the $sn100pn$ residual interaction in the $jj5pn$ model space [26] by using the shell-model code OXBASH [27]. As mentioned before, only an upper limit (<112 mb) was estimated for the inclusive one-neutron knockout cross section due to contaminants from the incoming beam. These contaminant events, though, can be efficiently removed by requiring γ-particle coincidence. After subtraction of the estimated feeding from higher-lying states, the exclusive first and higher-excited-state cross sections for knockout to ^{107}Sn were measured, providing a lower limit on the inclusive one (60 mb). For knockout to ^{107}Sn to the ground state we simply subtracted from the inclusive upper limit the measured exclusive cross sections (<52 mb). The sum of calculations to all shell-model final states above $N = 50$

TABLE I. Summary table of inclusive and exclusive neutron-removal cross sections from the ^{108}Sn beam. Cross sections using the shell-model spectroscopic factor (C^2S calculations from the $sn100pn$ residual interaction and the $jj5pn$ space are shown for comparison. The uncertainties shown include both statistical and systematic sources. The latter includes uncertainties on the particle identification of the incoming beam, reaction residues, and time of flight and position efficiencies.

Reaction	Final state	$C^2S_{\rm th}$	$\sigma_{\rm th}^{SM}$ (mb)	$\sigma_{\rm expt}$ (mb)
(^{108}Sn, ^{107}Sn)	$\frac{5}{2}^+$	2.52	19	<52
	$\frac{7}{2}^+$	3.42	16	11 ± 2
	via 1220 keV			49 ± 7
	$1h_{11/2}, 2d_{3/2}, 3s_{1/2}$	1.75	12	
	$1g_{9/2}$	1	~5[a]	
Inclusive (above $N = 50$)			48	
Inclusive (experimental)				<112

[a]For unit of single-particle strength.

having significant C^2S accounts for a total of 7.82 units of single-particle strength. Possible contributions from neutrons below $N = 50$ are not included but are estimated to contribute ≈5 mb per single-particle unit based on the single-particle cross sections for final states with excitation energy near the proton threshold. For knockout to ^{107}Sn in the $7/2^+$ state, the measured cross section is smaller than the calculation. According to our calculations, a small contribution to the cross section comes from ^{108}Sn ground-state configurations with valence neutrons in the $1h_{11/2}$, $2d_{3/2}$, and $3s_{1/2}$ orbitals, 7.5, 3.1, and 1.2 mb, respectively, accounting for a total of 1.75 units of single-particle strength. For the the $1g_{9/2}$ orbital, the first below the $N = 50$ gap, the calculated cross section is ≈5 mb, corresponding to one unit of single-particle strength. From the results of this analysis, the total number of units from the $1g_{9/2}$ orbital that contribute to the inclusive cross section is unknown and may vary up to ten. The measured cross section to states decaying through the 1220 keV multiplet suggests that part of this is due to neutrons removed from below the $N = 50$ shell gap. The energy resolution of CAESAR is not sufficient to resolve possible, smaller contributions from transitions in the 3–4 MeV region from the γ background present in the spectrum. This may result in the discrepancy between the measured and calculated cross sections. For knockout to ^{107}Sn in the ground state, the measured upper limit is compatible with the calculations.

In summary, we determined the orbital angular momentum of the first-excited state of ^{107}Sn and deduce its spin and parity to be $7/2^+$. By exclusion, the ground state then is $J^\pi = 5/2^+$. The results follow the trend for light tin isotopes as predicted by shell-model calculations. We also measured an upper limit to inclusive and exclusive partial cross sections for one-neutron removal reactions to ^{107}Sn. The observed upper limit for the inclusive cross section is well above the calculated values. This can be explained as due to the removal of neutrons from below the $N = 50$ shell gap and low statistics at high energies. The level scheme for ^{107}Sn has also been extended to excitation energies up to 5.5 MeV. These methods can be used for further spectroscopic studies toward ^{100}Sn.

This research was supported in part by the U.S. Department of Energy under Grants No. DE-SC0001174 and No. DE-FG02-96ER-40983, the National Science Foundation under Grants No. PHY-0757678, No. PHY-1102511, and No. PHY-1067906, and by the Basic Science Research Program through the National Research Foundation of Korea funded by the Ministry of Education, Science, and Technology under Grant No. NRF-2014S1A2A2028636. J. A. Tostevin acknowledges support from the Research Councils (UK) Grant No. ST/L005743/1. We also thank E. Simpson for the shell-model calculations and the A1900 group and the Cyclotron operators of the NSCL.

[1] M. G. Mayer and J. H. D. Jensen, in *Elementary Theory of Nuclear Shell Structure* (John Wiley and Sons, New York, NY, 1955).
[2] C. Engelmann *et al.*, Z. Phys. A: Hadrons Nucl. **352**, 351 (1995).
[3] P. T. Hosmer *et al.*, Phys. Rev. Lett. **94**, 112501 (2005).
[4] R. Schneider *et al.*, Z. Phys. A: Hadrons Nucl. **348**, 241 (1994).
[5] M. Lewitowicz *et al.*, Phys. Lett. B **332**, 20 (1994).
[6] R. K. Wallace and S. E. Woosley, Astrophys. J., Suppl. Ser. **45**, 389 (1981).
[7] D. D. DiJulio *et al.*, Eur. Phys. J. A **48**, 105 (2012).
[8] G. Guastalla *et al.*, Phys. Rev. Lett. **110**, 172501 (2013).
[9] V. M. Bader *et al.*, Phys. Rev. C **88**, 051301(R) (2013).
[10] D. Seweryniak *et al.*, Phys. Rev. Lett. **99**, 022504 (2007).
[11] I. G. Darby *et al.*, Phys. Rev. Lett. **105**, 162502 (2010).
[12] A. Gade *et al.*, Phys. Rev. C **77**, 044306 (2008).
[13] P. Hansen and B. Sherrill, Nucl. Phys. A **693**, 133 (2001).
[14] P. Hansen and J. Tostevin, Annu. Rev. Nucl. Part. Sci. **53**, 219 (2003).
[15] D. Morrissey *et al.*, Nucl. Instrum. Methods Phys. Res., Sect. B **B204**, 90 (2003).
[16] D. Bazin *et al.*, Nucl. Instrum. Methods Phys. Res., Sect. B **B204**, 629 (2003).
[17] D. Bazin *et al.*, Phys. Rev. Lett. **101**, 252501 (2008).
[18] D. Weisshaar *et al.*, Nucl. Instrum. Methods Phys. Res., Sect. A **A624**, 615 (2010).
[19] S. Agostinelli *et al.*, Nucl. Instrum. Methods Phys. Res., Sect. A **A506**, 250 (2003).
[20] K. L. Jones *et al.*, Acta Phys. Pol., B **46**, 537 (2015).
[21] M. Berz and K. Makino, *COSY INFINITY Version 8.1—Users Guide and Reference Manual*, Tech. Rep. (Michigan State University, East Lansing, MI, 2001).
[22] J. A. Tostevin and A. Gade, Phys. Rev. C **90**, 057602 (2014).
[23] S. R. Stroberg *et al.*, Phys. Rev. C **90**, 034301 (2014).
[24] H. Grawe, in *The Euroschool Lectures on Physics with Exotic Beams, Vol. I*, Lecture Notes in Physics (Springer, Berlin, Heidelberg, 2004), Vol. 651, pp. 33–75.
[25] J. A. Tostevin, J. Phys. G **25**, 735 (1999).
[26] B. A. Brown, N. J. Stone, J. R. Stone, I. S. Towner, and M. Hjorth-Jensen, Phys. Rev. C **71**, 044317 (2005).
[27] B. A. Brown *et al.*, *OXBASH for Windows*, MSU-NSCL Report 1289 (National Superconducting Cyclotron Laboratory, Michigan State University, East Lansing, MI, 2004).